IOP Publishing and International Atomic Energy Agency Nuclear Fusion
Nucl. Fusion **53** (2013) 013006 (10pp) doi:10.1088/0029-5515/53/1/013006

Fast-ion energy loss during TAE avalanches in the National Spherical Torus Experiment

E.D. Fredrickson[1], N.A. Crocker[1,2], D.S. Darrow[1], N.N. Gorelenkov[1], G.J. Kramer[1], S. Kubota[1,2], M. Podesta[1], R.B. White[1], A. Bortolon[1,3], S.P. Gerhardt[1], R.E. Bell[1], A. Diallo[1], B. LeBlanc[1], F.M. Levinton[1,4] and H. Yuh[1,4]

[1] Princeton Plasma Physics Laboratory, Princeton, NJ 08543, USA
[2] Department of Physics and Astronomy, University of California, Los Angeles, CA 90095, USA
[3] Department of Physics and Astronomy, University of California., Irvine, CA 92697, USA
[4] Nova Photonics, Princeton, NJ 08543, USA

Received 13 June 2012, accepted for publication 20 November 2012
Published 10 December 2012
Online at stacks.iop.org/NF/53/013006

Abstract
Strong toroidal Alfvén eigenmode (TAE) avalanches on NSTX, the National Spherical Torus Experiment (Ono *et al* 2000 *Nucl. Fusion* **40** 557) are typically correlated with drops in the neutron rate in the range 5–15%. In previous studies of avalanches in L-mode plasmas, these neutron drops were found to be consistent with modelled losses of fast ions. Here we expand the study to TAE avalanches in NSTX H-mode plasmas with improved analysis techniques. At the measured TAE mode amplitudes, simulations with the ORBIT code predict that fast ion losses are negligible. However, the simulations predict that the TAE scatter the fast ions in energy, resulting in a small (≈5–6%) drop in fast ion β. The net decrease in energy of the fast ions is sufficient to account for about 50% of the drop in neutron rate, redistribution for ≈40%, and fast ion losses account for only ≈10%. This loss of energy from the fast ion population is comparable to the estimated energy lost by damping from the Alfvén wave during the burst. The previously studied TAE avalanches in L-mode are re-evaluated using an improved calculation of the potential fluctuations in the ORBIT code near the separatrix.

1. Introduction

The National Spherical Torus Experiment (NSTX) is a medium size (major radius ≈0.85 m, minor radius ≈0.65 m), low aspect ratio tokamak capable of toroidal fields up to 5.6 kG and plasma currents up to 1.4 MA [1]. The plasma can be heated with up to 6 MW of deuterium neutral beams, which are injected with energies from ≈65 keV up to 90 keV. At these energies, the beam ion velocities can be several times the Alfvén velocity over the typical ranges of plasma density and magnetic field.

The super-Alfvénic fast ion population routinely excites a broad spectrum of MHD and Alfvénic mode activity (figure 1(*a*)), extending from low-frequency (<50 kHz) fishbone and other kink-like modes [2–7], toroidal Alfvén eigenmodes (TAEs) [8–12], up to compressional and global Alfvén modes [13–27] with frequencies up to ≈2.5 MHz and occasionally at even higher frequencies. Similar Alfvénic instabilities have also been extensively studied on the beam-heated START and MAST devices [28–39]. TAEs were, of course, discovered in conventional beam and ICRF heated tokamaks [40–49]. Experimental and theoretical efforts are underway to characterize these various modes, understand the mechanisms for excitation of the modes, how apparently disparate modes interact [9, 12], and the effect that the multiple modes have on the fast ion population. For example, the TAE avalanches shown here appear to be triggered by avalanches of GAE near 800 kHz [50].

In this paper, we report on benchmarking of the guiding centre code ORBIT [51] for modelling fast ion transport. The ORBIT simulations use the experimentally measured mode amplitude and frequency evolutions, combined with linear eigenmodes calculated with the ideal stability code, NOVA (and NOVA-k) [52, 53]. Similar benchmarking has been performed previously on DIII-D [54, 55], as well as comparisons of self-consistent, non-linear code predictions with experimental data [56, 57]. Recent analysis of NSTX and DIII-D data [55, 58] has demonstrated the importance to fast ion transport of the perturbed electric field from TAE.

The potential fluctuations are calculated in ORBIT by assuming that the parallel electric field, $E_\parallel = 0$ or

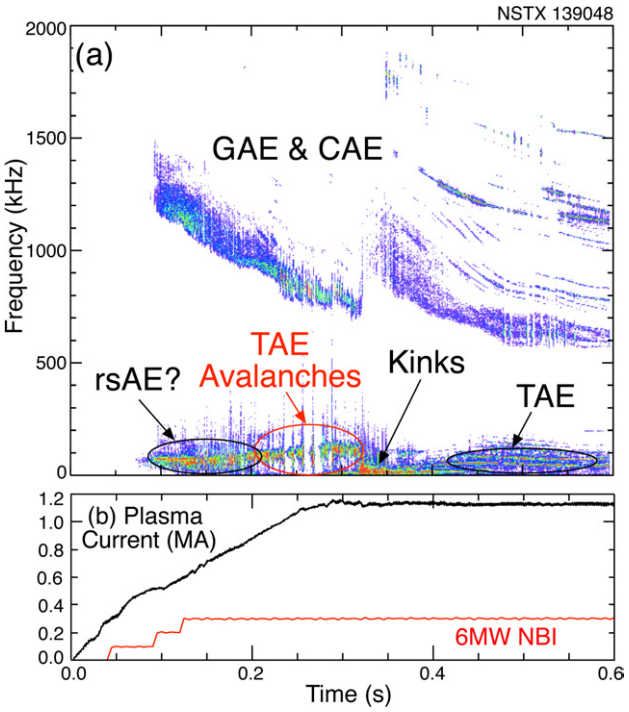

Figure 1. (*a*) Spectrogram of magnetic fluctuations, (*b*) plasma current and neutral beam power evolution.

$\phi_{m,n} = \omega A_{\|}^{m.n}/k_{\|}^{m,n}$. However, $k_{\|}^{m,n} = 0$, and $A_{\|}^{m,m} = 0$, at the rational surface, which causes numerical problems as the zeros of $A_{\|}$ and $k_{\|}$ cannot be perfectly aligned. These problems can be alleviated, but not eliminated, by tricks like replacing $A_{\|}/k_{\|}$ with $k_{\|}A_{\|}/(k_{\|}^2+\varepsilon)$ as in [54, 55, 58]. However, this can introduce large spikes in the radial electric field, particularly if the zeros in $A_{\|}$ and $k_{\|}$ do not perfectly align. The version of ORBIT used here interpolates the slowly varying potential across the rational surface, and also better aligns the zeros of $A_{\|}$ and $k_{\|}$.

The TAEs in NSTX are seen in a broad range of beam-heated plasma regimes, but most commonly in plasmas with lower density, hence relatively larger fast ion populations (e.g., in equilibrium $\beta_{\rm fast}/\beta_{\rm thermal} = \tau_{\rm slow}/\tau_E$, thus higher temperature, lower density plasmas tend to have a higher $\beta_{\rm fast}/\beta_{\rm thermal}$). The parameter, $\beta_{\rm fast}/\beta_{\rm thermal}$, serves as a proxy for the ratio of drive ($\beta_{\rm fast}$) to damping ($\beta_{\rm thermal}$). The dimensionless parameter, $V_{\rm fast}/V_{\rm Alfvén}$ is a measure of the fraction of the non-thermal fast ion population that can satisfy the resonance conditions. Finally, the normalized fast ion Larmor radius, $\rho_{\rm fast}/a$ is a measure of how effectively the TAE can transport the fast ions across the plasma cross-section. These parameters for a typical ITER-like operating point [59] and for the NSTX H-mode discussed here are compared in table 1. While some of the NSTX parameters are significantly different than those for the ITER operating point (except for the ratio of $V_{\rm fast}$ to $V_{\rm Alfvén}$), these data still provide a good test of the codes used to predict TAE-induced fast ion transport in ITER. Of course, NSTX fast ion parameters are likely more similar to those for a next-step DT spherical tokamak, but those operating points are far less certain, thus more uncertain to compare with, than the ITER operating points.

Typically the density is too high in NSTX H-modes, and the density profile is too flat, for mode measurements with the reflectometers. Previous simulations of fast ion losses with the ORBIT code for TAE avalanches on NSTX were done using data from L-mode plasmas [8–12]. The measured mode amplitude was found to be in approximate agreement with the threshold for fast ion losses [58]. In this paper we extend the investigation of TAE mode avalanches to low density H-mode plasmas, and apply the improved analysis techniques to the previously analysed L-mode TAE avalanches.

Table 1. Comparison of some relevant parameters for a typical ITER-like plasma and the NSTX parameters for the H-mode shot. (NSTX $V_{\rm fast}/V_{\rm Alfvén}$ is edge to centre).

	ITER	NSTX
$V_{\rm fast}/V_{\rm Alfvén}$	1.86	1.6–2.5
$\langle\beta_{\rm fast}\rangle/\langle\beta_{\rm thermal}\rangle$	0.54	1.64
$\rho_{\rm fast}/a$	0.026	0.23
$T_{\rm e}(0)$ (keV)	23.5	1.1
$n_{\rm e}(0)$ (10^{19} m^{-3})	10.2	2.8

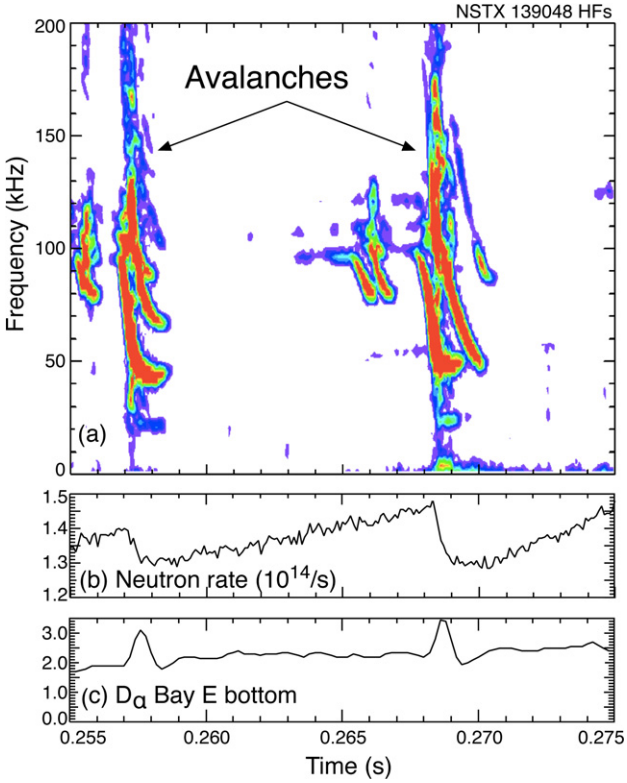

Figure 2. (*a*) Spectrogram of magnetic fluctuations showing two TAE avalanche bursts, (*b*) neutron rate drops at each burst (note suppressed zero), (*c*) Dα spikes at bursts.

In figure 1(*a*) we show a spectrogram of magnetic fluctuations for a low density H-mode plasma with moderate density peaking where TAE avalanching is present from roughly 0.2 to 0.35 s. The time history of plasma current and neutral beam power are shown in figure 1(*b*). The beams are injected with three sources, each providing 2 MW of deuterium beams at a full-energy of 90 keV. The three beam sources are injected co-tangentially with tangency radii of 0.497 m, 0.592 m and 0.694 m, respectively.

The magnetic fluctuation spectrogram in figure 1(*a*) is expanded in figure 2(*a*) showing TAE avalanches at ≈0.259 s and ≈0.268 s. As is typical, the TAE occur as a sequence

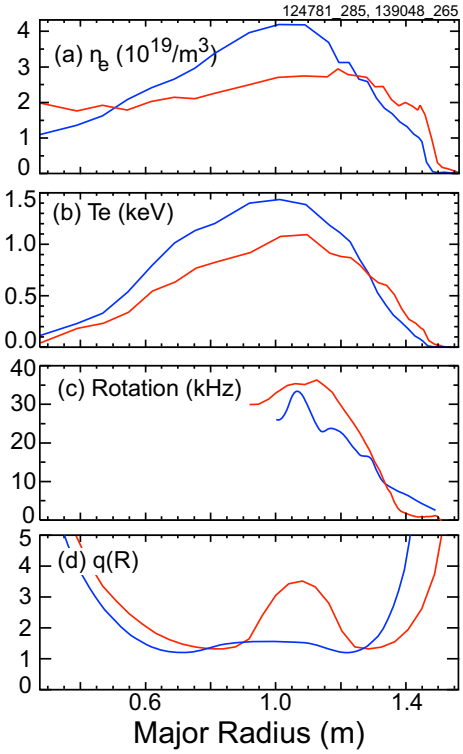

Figure 3. Profiles of (*a*) density, (*b*) electron temperature, (*c*) rotation velocity and (*d*) q for the H-mode (red) and L-mode (blue).

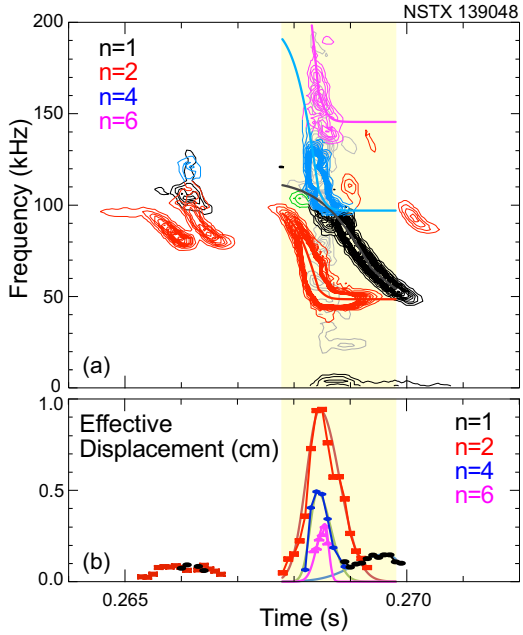

Figure 4. (*a*) Spectrogram of a Mirnov coil where contours are colour-coded to indicate the toroidal mode numbers, as indicated in the legend, (*b*) the peak mode amplitude evolution for each mode from the reflectometer array.

of bursts, with each burst chirping downward in frequency (figure 2(*a*)). Drops in the neutron rate of 7% and 12% are seen to be correlated with the TAE avalanches in figure 2(*b*). The neutron rate ramps up nearly linearly between avalanches, suggesting that the next avalanche is triggered before the fast ion population reaches equilibrium. In figure 2(*c*), spikes in D-alpha light coincident with the avalanches suggest losses of beam ions.

In figure 3 profiles versus major radius of some important plasma parameters for this H-mode shot (red) and the previously analysed L-mode shot (blue) during the avalanching period are shown. The central density is lower and the profile less peaked (figure 3(*a*)). The electron temperatures are comparable in both shots (figure 3(*b*)). In principle, the broader density profile would lead to a different TAE gap, or continuum, structure, but here the gap structure is mainly influenced by the strongly sheared toroidal rotation (figure 3(*c*)), similar in both shots. Both show shear reversal in the q-profile, with the H-mode having stronger shear reversal (figure 3(*d*)). The q-profiles were reconstructed using motional Stark effect measurements of the magnetic field pitch angle [60] and the LRDFIT equilibrium code [61].

The TAE avalanches provide an opportunity to validate codes used for modelling fast ion transport. The process begins with equilibrium reconstruction and TRANSP [62] runs to validate the kinetic data and simulate beam deposition. The TAEs are characterized with Mirnov coil arrays which measure the toroidal mode numbers and with a reflectometer array which provides an absolute, internal measurement of the mode amplitude evolution, as well as some information on the radial structure of the modes [63]. The ideal, fixed boundary, NOVA-k code is used to model the eigenmode structures and to predict the linear growth and damping rates. The NOVA eigenmodes which best fit the experimental mode profiles measured with the reflectometer array are then imported into the ORBIT code, together with the experimentally measured amplitude and frequency evolutions. The ORBIT simulations use a representative sample of fast ions from the fast-ion slowing-down distribution function calculated in TRANSP. Typically 4000 particles are sufficient to give reasonable statistics on variations in neutron rates and particle losses for the avalanches analysed here.

In this paper we focus primarily on the ORBIT simulations. The analysis of experimental data and the NOVA simulations were discussed in detail previously [58].

2. TAE avalanches in H-mode plasmas

The modelling of fast ion losses from TAE avalanches begins with the measurement of the toroidal mode numbers using a toroidal array of Mirnov coils. A spectrogram of a Mirnov coil signal of the avalanche at 0.268 s is shown in figure 4(*a*) where toroidal mode #'s are indicated by the contour colours. There are four important modes in the final avalanche burst (region indicated in yellow), beginning with the strong growth of an $n = 2$ TAE (red contours). The $n = 4$ and $n = 6$ modes appear strongly coupled to the $n = 2$ mode in that the frequency evolutions of the $n = 4$ and 6 modes (blue and magenta contours, respectively) are nearly harmonics of the $n = 2$ mode. An $n = 1$ TAE appears towards the end of the burst. The amplitude evolution of these four modes as measured with the three innermost reflectometer channels are shown in figure 4(*b*). The frequency and amplitude data is fit with analytic formulas for each mode, shown by the solid curves in figures 4(*a*) and (*b*), which are used in the

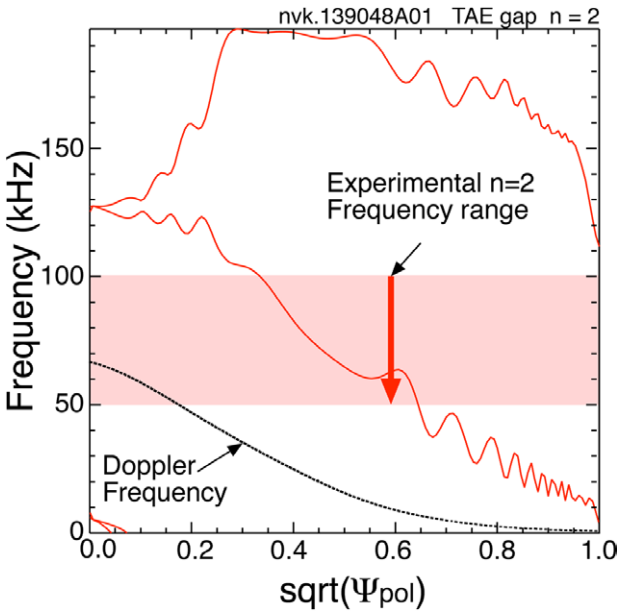

Figure 5. The continuum structure for the $n = 2$ TAE including the experimental sheared rotation profile. The red band shows the range of the $n = 2$ TAE frequency chirp.

ORBIT code simulations described below. The ORBIT code simulations cover about 2 ms (yellow region, figure 4). There are two weaker bursts of modes prior to the final avalanche burst. These modes, as is typical, are roughly a factor of ten lower in amplitude.

2.1. Simulation with NOVA and ORBIT of fast ion transport by TAE

The linear eigenmodes for each of the four dominant modes in figure 4 are calculated with NOVA using the plasma equilibrium as input. Strong, sheared, plasma toroidal rotation greatly affects the structure of the TAE continuum, as seen in figure 5. The eigenmodes are calculated with a version of NOVA which includes some of the physics due to the sheared rotation. This is particularly important in low aspect ratio tokamaks where the low field results in a relatively low frequency for the TAE, but strong, co-tangential neutral beam injection spins the plasma at frequencies higher, in some cases, than the TAE frequency. In the gap structure shown in figure 5 for the $n = 2$ mode, it is seen that the TAE frequency at mode onset intersects the continuum, and towards the end of the frequency chirp is of order zero in the plasma frame near the axis. This raises important physics issues concerning the coupling of TAE to MHD modes, such as kinks [9, 12]. In practice, it also means that the TAE gap is generally closed on NSTX, that is that the mode stability should not be strongly affected by changes either in the q-profile or the density profile. In fact, quite often the TAE chirp down in frequency from ≈100 kHz to ≈50 kHz, which might normally be expected to move the TAE from the gap to strong continuum interactions, yet no significant change is seen in the mode evolution.

The NOVA calculation of the eigenmodes is linear and these eigenmodes need to be scaled with the experimental measurements to be used in the ORBIT code. The process determines the absolute mode amplitude by simulating the reflectometer response to the eigenmode structure, and scaling the linear eigenmodes to match the absolute reflectometer measurements (which are not a directly local measurement of the mode amplitude) for each of the TAE. Figures 6(*a*)–(*d*) show comparisons of the simulated reflectometer responses (black curves) compared to the experimental measurements. The insets show the dominant poloidal harmonics in Boozer coordinates.

For the $n = 2$ and $n = 4$ modes, the agreement with the shape is reasonable. The measured profiles of the $n = 1$ and $n = 6$ modes have larger amplitude towards the edge than the NOVA simulations, which were found using a conducting boundary at the plasma surface, thus the mode structure near the plasma edge is not well reproduced. However, with only a finite number of poloidal harmonics NOVA cannot in any case resolve the eigenmode structure near the separatrix. Here, the eigenmode radial shapes were fit with only 14 poloidal harmonics. For these reasons, and others, this work should be viewed as a somewhat qualitative, rather than quantitative, study.

An important effect of the TAE avalanche in the ORBIT simulation is to reduce the net energy of confined beam ions by ≈5.4%, as shown in figure 7 (only fast ions with energy greater than 20 keV were included in the ORBIT simulation). Each blue point represents a beam ion in the ORBIT simulation; those points near the red line have nearly the same initial and final energy (although the energy could have varied through the simulation). At the measured mode amplitude, the fast ions are scattered by ≈±10 keV, with a net loss of fast ion energy of ≈5.4%. Approximately 3% of the fast ions are lost in the simulation using the experimental mode amplitudes.

2.2. Estimate of change in neutron rate

The change in neutron rate, S, is estimated for the perturbed fast ion distribution using the energy-dependence of the fusion cross-section, together with the drop in fusion rate from radial redistribution of beam ions to lower density plasma regions and beam ion losses [54]. There is a net estimated drop in the neutron rate of ≈23%, larger than the measured drop of ≈12% for the ORBIT simulations using the measured mode amplitude.

The scaling of the simulated neutron rate drop with TAE amplitude is shown in figure 8. Simulations are done with the measured mode amplitude scaled by factors ranging from 0.1 up to 2.5. Up to the measured mode amplitude (normalized mode amplitude of one), the neutron drop is primarily from the redistribution of fast ions to lower plasma density regions and loss of energy from the fast ions. Above that amplitude, the losses of fast ions become the dominant mechanism for the drop in neutron rate. The experimental neutron rate drop of ≈12% is seen at ≈0.7 times the measured mode amplitude. For the simulation with normalized mode amplitude of 0.7, ≈52% of the neutron drop is due to the change in fast ion energy, ≈39% is from redistribution of fast ions to lower density regions of the plasma (flattening of the fast ion profile), and ≈9% is from loss of fast ions. (The change in neutron rate due only to fast ion energy change is calculated by introducing a flat target density profile, thus redistribution of fast ions does not affect the neutron rate.) Here, lost means guiding centre

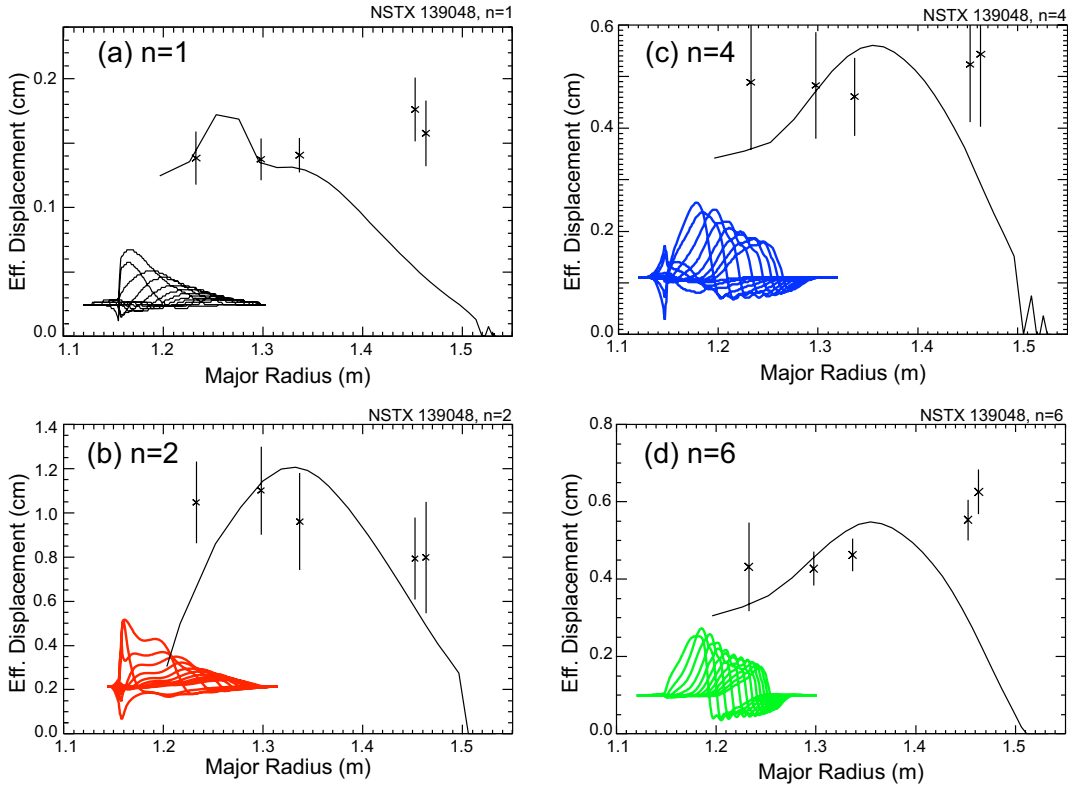

Figure 6. Solid curves are simulated reflectometer response, points are reflectometer data, the inset are NOVA poloidal harmonics for (*a*) $n = 1$ mode, (*b*) $n = 2$ mode, (*c*) $n = 4$ mode and (*d*) $n = 6$ mode.

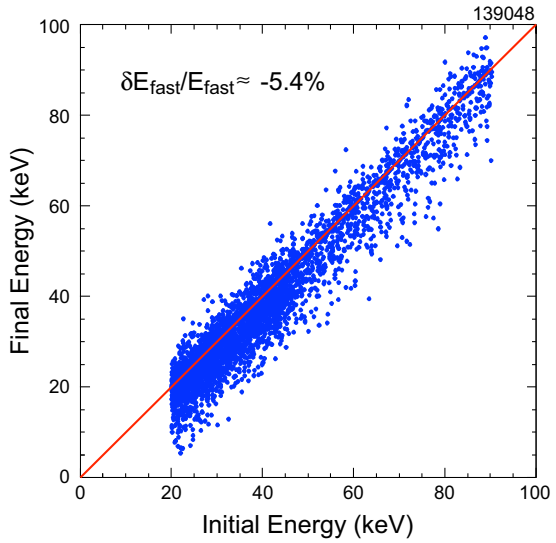

Figure 7. Initial and final beam ion energies for an ORBIT simulation using measured mode amplitude and frequency evolutions.

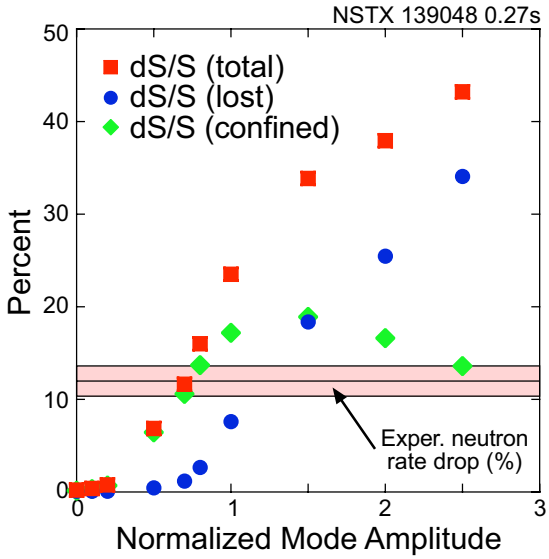

Figure 8. Total neutron rate drop versus scaled TAE amplitude (red squares), for the confined fast ion population (green diamonds) and due only to fast ion losses (blue circles).

orbits which cross the last closed flux surface, which may tend to overestimate losses, as many of these fast ions will re-enter the plasma. However, a more accurate treatment of mode amplitudes near the edge in ORBIT might enhance losses.

The change in neutron rate between the initial and final fast ion distributions is calculated separately for the beam–beam and beam–target neutron contributions. The beam–target fusion rate is proportional to $n_{\rm ion} n_{\rm b} \sigma(E_{\rm b}) v_{\rm b}$ where $n_{\rm ion}$ and $n_{\rm b}$ are the local thermal and beam deuterium densities, σ is the energy-dependent fusion cross-section, and $E_{\rm b}$ and $v_{\rm b}$ are the energy and velocity of the beam ion, respectively. Then, taking the fast ion distribution in ORBIT as representative, the beam–target neutron rate will be proportional to

$$S^{\rm B-T} \approx \sum_{i=1}^{N} n_{\rm ion}(\psi_i)\sigma(E_i)v_i,$$

where the sum is over the sample fast ion distribution used in ORBIT and $n_{\rm ion}(\psi_i)$ is the thermal deuterium ion density near each beam ion. The sum is done for the initial fast ion distribution, $S^{\rm Initial}$, and the final fast ion distribution, $S^{\rm Final}$, where $S^{\rm Final}$ also includes the drop in neutron rate from beam ions that were lost. These are not absolute neutron rates, so the relative change is reported as $\delta S^{\rm B-T}/S^{\rm B-T} \approx (S^{\rm Initial} - S^{\rm Final})/S^{\rm Initial}$.

Estimating the drop of the neutron rate for beam–beam reactions is more difficult. Determining the effective fusion cross-section in the rest frame of one of the fast ions is complicated. However, for a Maxwellian distribution of energetic deuterium ions, with a temperature of 50 keV, the fusion rate increases approximately linearly with temperature [64]. While the beam ion slowing-down distribution is neither Maxwellian, nor isotropic, a linear dependence on energy may not be an unreasonable approximation for the fusion cross-section energy dependence. The beam–beam fusion rate is then roughly proportional to $n_{\rm b} n_{\rm b} E_{\rm b} v_{\rm b}$ and the beam–beam fusion rate is then proportional to

$$S^{\rm B-B} \approx \sum_{i=1}^{N} n_{\rm b}(\psi_i) E_i v_i$$

and the change is calculated, as for the beam–target rate above, as $\delta S^{\rm B-B}/S^{\rm B-B} \approx (S^{\rm Initial} - S^{\rm Final})/S^{\rm Initial}$. In this shot, TRANSP calculations find that 25% of the neutron rate is from beam–beam reactions, 75% from beam–target so for this shot $\delta S^{\rm total}/S^{\rm total} = 0.75\delta S^{\rm B-T}/S^{\rm B-T} + 0.25\delta S^{\rm B-B}/S^{\rm B-B}$.

2.3. *Investigation of power flow through TAE*

The ORBIT simulations predict that for a neutron rate drop of 12%, there is a corresponding drop of about 3.6% of the fast ion energy (and 0.6% of fast ions lost). This energy is presumed to go to the TAE, and can be compared with an estimate of the energy transferred from the TAE burst to the thermal plasma through wave damping. The energy in the wave is estimated as twice the magnetic fluctuation energy, and the magnetic fluctuation energy is estimated as twice the radial magnetic fluctuation energy (to account for the energy in the poloidal magnetic field fluctuations). Thus, normalized to the magnetic field energy, $\beta_{\rm wave} \approx 4(\delta B_r/B)^2$. The peak wave field, $\beta_{\rm wave}$, volume averaged using the NOVA 2D eigenmodes, is $\approx\langle 4(\delta B_r/B)^2\rangle_{\rm vol} \approx 1.9 \times 10^{-4}$. The fast ion beta is 2.9×10^{-2}, and the change in fast ion beta, $\delta\beta_{\rm fast} \approx 1.0\times10^{-3}$. Thus, $\delta\beta_{\rm fast}/\beta_{\rm wave} \approx 5.3$, or roughly five times as much energy was lost from the fast ions as was present at peak amplitude in the mode. This estimate of the energy flowing from the fast ions to the TAE will be compared with an estimate of the energy lost from the TAE to the thermal plasma throughout the burst, using an experimentally estimated damping rate, as discussed below. If ion Landau damping is much larger than continuum or electron collisional damping, this could provide a mechanism for 'alpha-channelling' of fusion-alpha energy [65] to the thermal ions in a reactor. However, even for these relatively large modes the fraction of beam power estimated to be moving through the TAE is very small, $\ll$1%.

The ratio of the net energy lost to the thermal plasma by damping of the wave to the peak energy in the wave can be estimated analytically from the wave amplitude evolution and the linear damping rate. The amplitude evolution of the burst can be roughly fit with a Gaussian shape in time, as shown in figure 9. The energy lost through damping can then be estimated from the integral of wave energy times the damping rate over the burst.

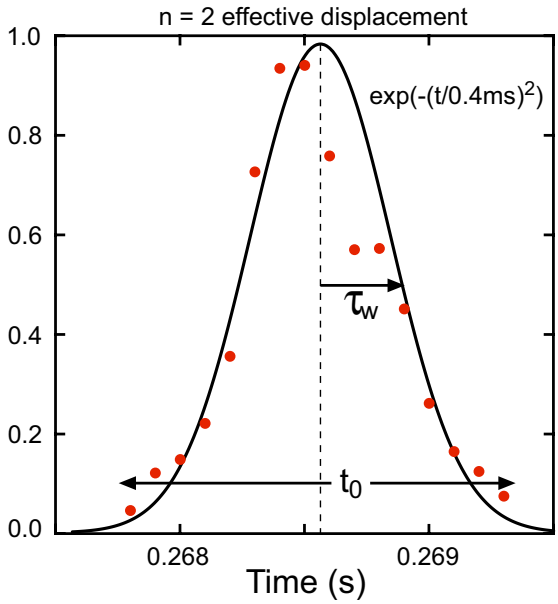

Figure 9. Experimental $n = 2$ mode amplitude from reflectometer array (red points), Gaussian approximation (solid line).

$$W_{\rm loss}/W_{\rm peak} = 2\gamma_{\rm damp}\int_{-t_0/2}^{t_0/2}\exp(-2(t/\tau_w)^2)\,{\rm d}t$$
$$\approx 2\gamma_{\rm damp}\int_{-\infty}^{\infty}\exp(-2(t/\tau_w)^2)\,{\rm d}t = \sqrt{2\pi}\gamma_{\rm damp}\tau_w.$$

Here, $\tau_w = 0.4$ ms is the effective width of the TAE burst, $2\gamma_{\rm damp}$ is the linear energy damping rate and t_0 is roughly the duration of the burst. The damping rate can be estimated by fitting the mode decay rate, which would tend to underestimate the actual damping rate as some drive may still be present. A fit gives a damping rate of $\gamma_{\rm damp} > 3.8\,{\rm ms}^{-1}$, or $\gamma_{\rm damp}/\omega \approx 0.6\%$. Alternatively, a Gaussian amplitude evolution for a burst can be modelled with a constant damping rate and a linearly decreasing drive term over the period of the burst which gives a second empirical estimate for the damping rate. Over a period from $-t_0/2 \leqslant t \leqslant t_0/2$, where $t_0 \approx 1.6$ ms, the growth rate can be modelled as

$$\gamma(t) = \gamma_{\rm drive} - \gamma_{\rm damp} = (\gamma_{\rm damp} - 2\gamma_{\rm damp}t/t_0) - \gamma_{\rm damp}$$
$$= -2\gamma_{\rm damp}t/t_0.$$

The mode amplitude evolution is then

$$A(t) = \exp\left(\int_{-t_0/2}^{t_0/2} -2\gamma_{\rm damp}(t/t_0)\,{\rm d}t\right)$$
$$= \exp(-\gamma_{\rm damp}t_0(t/t_0)^2).$$

The damping rate can be found by comparing to the Gaussian fit shown in figure 9, from which we find $\gamma_{\rm damp} \approx 10\,{\rm ms}^{-1}$, or $\gamma_{\rm damp}/\omega \approx 1.6\%$. (Both empirical estimates are somewhat less than the NOVA-k estimate of the $n = 2$ mode ion Landau damping of $\gamma_{\rm ion}/\omega \approx 2.1\%$, and including electron collisional and radiative damping would increase the NOVA-k estimated

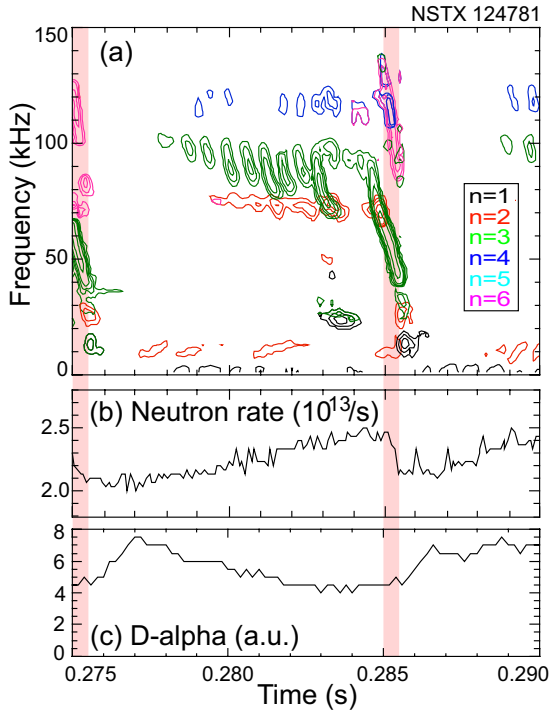

Figure 10. (*a*) Spectrogram of magnetic fluctuations showing two TAE avalanche bursts, (*b*) neutron rate drops at each burst, (*c*) Dα spikes at bursts.

damping rate.) Using the empirically determined damping rates, the ratio $W_{\rm loss}/W_{\rm peak} \approx 4$ to 10, so the energy lost from the fast ion population in the ORBIT simulations is in qualitative agreement with the experimental estimates for mode amplitude evolution and damping.

Avalanches in L-mode plasmas. A previous study of fast ion losses from TAE avalanches in L-mode plasmas was described in [58]. The avalanche data were revisited using the updated ORBIT code and analysis techniques employed in the above work.

One of the L-mode TAE avalanches is seen in the spectrogram of magnetic fluctuations shown in figure 10(*a*). The dominant mode in this case was an $n = 3$ TAE (green contour). There were also weaker $n = 2$, 4 and 6 TAE in the avalanche burst. The burst itself was only ≈1 ms in duration, shorter than the H-mode case. The drop in the neutron rate was comparable at ≈12% (figure 10(*b*)). The D-alpha data suggest fast ions were lost as in the H-mode case (figure 10(*c*)).

The original choice to study TAE avalanches in L-mode plasmas was motivated by the improved reflectometer measurements of the mode structure with a peaked density profile. Producing TAE avalanches in L-mode requires lower voltage neutral beams, for reasons not understood at this time. A helium pre-fill and gas puffing were used to suppress the H-mode transition. Both the helium content of the plasma and the reduced beam voltage led to a significantly lower neutron rate in the L-mode case.

In the previous analysis [58], the reflectometer data were modelled using only the displacement contribution to the density perturbation. The compressional contribution was approximately modelled by scaling the displacement density perturbation. Here, the reflectometer data have been modelled explicitly using the compressional and displacement terms, which results in only modest changes to the mode amplitudes used in ORBIT. The fits are generally better than in the H-mode case (figure 11). Both NOVA and the experimental measurements suggest that the TAE were more core localized than in the H-mode. The $n = 6$ mode has also been included, although the impact of that was modest. The new fits to the reflectometer array data are shown in figure 11.

The largest change in the new analysis is that ORBIT has a more accurate calculation of the electric field from the TAE near the rational surfaces. With the more accurate representation of the electric field, fewer fast ion losses are seen in the simulations compared with [58]. However, the reduction in the simulated neutron rate is largely compensated by the recognition of neutron rate drop due to energy loss which was neglected in [58]. In figure 12 the net neutron rate drop in ORBIT simulations (red squares), the neutron drop due to lost beam ions (blue circles) and neutron drop in the confined beam ion population due to fast ion redistribution and loss of energy to the TAE are shown. As above, the change in neutron rates are calculated for beam–target and beam–beam neutrons, and those two calculations are combined using the TRANSP prediction that ≈63% of the neutron rate is from beam–beam reactions and only ≈37% are beam–target. The lower beam–target neutron rate from the reduced beam voltage and nominal He target plasma results in a larger percentage of beam–beam neutrons.

As was the case in the H-mode avalanches analysed above, there is an apparent threshold for energy loss in the fast ion population at a normalized mode amplitude of ≈0.4, and the threshold for fast ion loss onset occurs at a normalized mode amplitude of ≈1. There is good agreement between the measured neutron rate drop and that predicted at the measured mode amplitude. The previous analysis only estimated the neutron rate drop due to fast ion losses. This analysis predicts smaller fast ion losses, but including the neutron rate reduction from redistribution and energy loss results in a similar predicted neutron rate drop, close to the experimental observation.

3. Summary and discussion

Simulations of fast ion transport due to TAE avalanches in NSTX are in qualitative agreement with experimental data. A surprising result is that ORBIT simulations predict small fast ion losses up to the measured mode amplitudes, however fast ion redistribution and the energy taken from the fast ions by the TAE is sufficient to reduce the neutron rate as experimentally observed. The perturbation to the beam–target neutron rate is estimated using the change to the fast ion distribution function and the beam–target fusion cross-section and target deuterium density. The calculation of the change to the beam–beam rate is more complicated, so a simple estimate is made based on the change in the effective temperature (energy) in the slowing-down distribution. The scaling and magnitude of the beam–beam and beam–target rate changes are found to be roughly comparable, and the sum is in qualitative agreement with the measured neutron rate change.

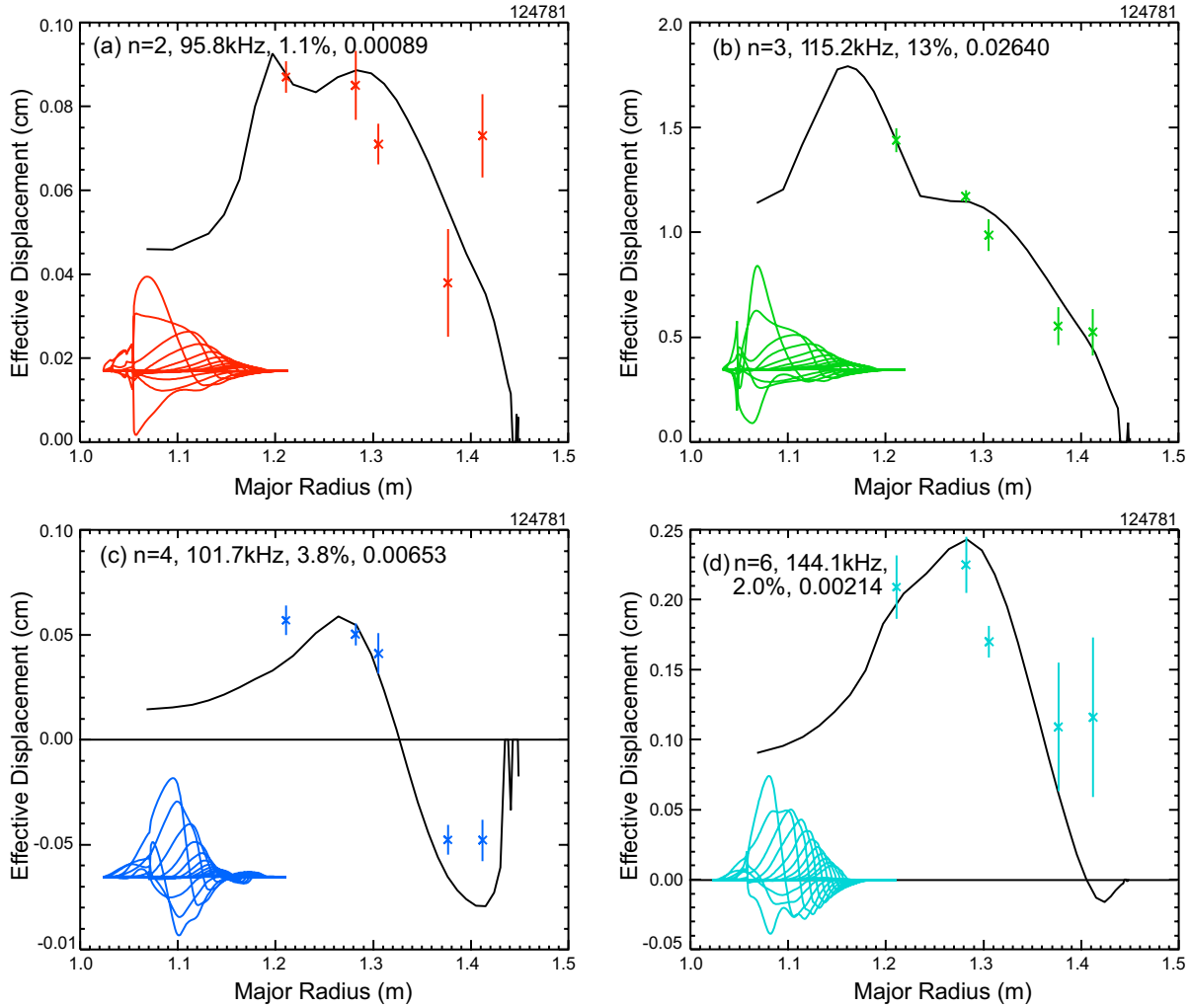

Figure 11. Solid curves are the simulated reflectometer response, points are reflectometer data, inset are NOVA poloidal harmonics for (*a*) $n = 2$ mode, (*b*) $n = 3$ mode, (*c*) $n = 4$ mode and (*d*) $n = 6$ mode.

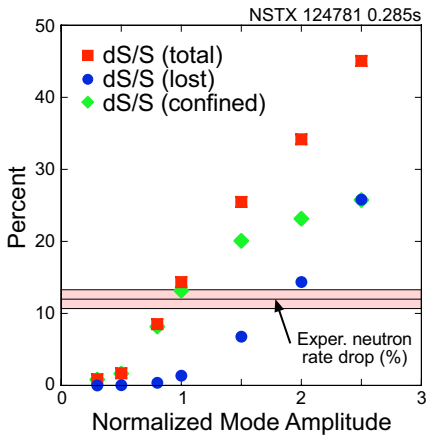

Figure 12. Simulated neutron rate drop due to TAE avalanche (red), neutron rate drop resulting from lost beam ions (blue) and neutron rate drop in confined beam ion population from energy loss (green).

The simulations of the new TAE H-mode avalanches were done with a version of ORBIT where the potential fluctuations from the mode near rational surfaces were more accurately calculated. Application of ORBIT with the improved potential fluctuation calculation, and some refinements in the input of mode structure to ORBIT, found a different result than the previous analysis [58]. Then, fast ion losses alone were sufficient to explain the observed neutron drop. The analysis with the improved calculation of the electric field finds very low levels of fast ion loss at observed mode amplitudes in the previously studied L-mode, but fast ion redistribution and the loss of fast ion energy is sufficient to account for the observed neutron drop.

The simulations of the TAE avalanches in the L-mode case are in good agreement with experiment. However, in the H-mode case the mode amplitudes needed reduction by ≈0.7 to get agreement with the observed neutron rate drop. At some level it is surprising that the agreement is as good as it is. The use of the ideal eigenmodes, with unphysical interactions with the continuum, the use of the unperturbed fast ion distributions in the presence of multiple Alfvénic instabilities, the use of a guiding centre code in a situation with large larmor radii, together with the general uncertainties in equilibrium reconstruction could all potentially contribute to large uncertainty in the simulations. Future experiments with improved diagnostics and more advanced analysis codes

will continue to investigate our understanding of fast ion confinement.

Acknowledgment

Work supported by US DOE Contracts DE-AC02-09CH11466, DE-FG03-99ER54527, DE-FG02-06ER54867 and DE-FG02-99ER54527.

References

[1] Ono M. *et al* and the NSTX Team 2000 *Nucl. Fusion* **40** 557
[2] White R.B. *et al* 1983 *Phys. Fluids* **26** 2958
[3] Kaita R., White R.B., Morris A.W., Fredrickson E.D., McGuire K.M., Medley S.S., Murphy T.J. and Scott S.D. 1990 *Phys. Fluids* B **2** 1584
[4] Heidbrink W.W. 1995 Beam-driven chirping instability in DIII-D *Plasma Phys. Control. Fusion* **37** 937
[5] Fredrickson E.D., Chen L. and White R.B. 2003 Bounce precession fishbones in the National Spherical Torus Experiment *Nucl. Fusion* **43** 1258
[6] Darrow D.S. *et al* 2002 Measurements of prompt and MHD-induced fast ion loss from National Spherical Torus Experiment plasma *Proc. 19th Int. Conf. on Fusion Energy 2002 (Lyon, France, 2002) (Vienna: IAEA)* CD-ROM file (EX/P2-01) and www.iaea.org/programmes/ripc/physics/fec2002/html/fec2002.htm
[7] Kolesnichenko Ya.I., Marchenko V.S. and White R.B. 2006 *Phys. Plasmas* **13** 052504
[8] Fredrickson E.D., Gorelenkov N.N., Bell R.E., Menard J.E., Roquemore A.L., Kubota S., Crocker N.A. and Peebles W. 2006 Fast ion loss in a 'sea-of-TAE' *Nucl. Fusion* **46** s926
[9] Crocker N.A., Peebles W.A., Kubota S., Fredrickson E.D., Kaye S.M., LeBlanc B.P. and Menard J.E. 2006 Three-wave interactions between fast-ion modes in the National Spherical Torus Experiment *Phys. Rev. Lett.* **97** 045002
[10] Podestà M. *et al* 2009 Experimental studies on fast-ion transport by Alfvèn wave avalanches on the National Spherical Torus Experiment *Phys. Plasmas* **16** 056104
[11] Podestà M., Bell R.E., Fredrickson E.D., Gorelenkov N.N., LeBlanc B.P., Heidbrink W.W., Crocker N.A., Kubota S. and Yuh H. 2010 Effects of toroidal rotation shear on toroidicity-induced Alfvèn eigenmodes in the National Spherical Torus Experiment *Phys. Plasmas* **17** 122501
[12] Podestá M., Bell R.E., Crocker N.A., Fredrickson E.D., Gorelenkov N.N., Heidbrink W.W., Kubota S., LeBlanc B.P. and Yuh H. 2011 Non-linear dynamics of toroidicity-induced Alfvén eigenmodes on the National Spherical Torus Experiment *Nucl. Fusion* **51** 063035
[13] Gorelenkov N.N. and Cheng C.Z. 1995 *Phys. Plasmas* **2** 1961
[14] Fredrickson E.D. *et al* 2001 *Phys. Rev. Lett.* **87** 145001
[15] Gorelenkov N.N., Cheng C.Z. and Fredrickson E. 2002 Compressional Alfven eigenmode dispersion in low aspect ratio plasmas *Phys. Plasmas* **9** 3483
[16] Fredrickson E.D. *et al* 2002 *Phys. Plasmas* **9** 2069
[17] Gorelenkov N.N., Cheng C.Z., Fredrickson E., Belova E., Gates D., Kaye S., Kramer G.J., Nazikian R. and White R.B. 2002 Compressional Alfvén eigenmode instability in NSTX *Nucl. Fusion* **42** 977
[18] Gorelenkov N.N., Fredrickson E., Belova E., Cheng C.Z., Gates D., Kaye S. and White R.B. 2002 Theory and observation of compressional Alfvén eigenmodes in low aspect ratio plasma *Proc. 19th Int. Conf. on Fusion Energy 2002 (Lyon, France, 2002)* (Vienna: IAEA) CD-ROM file TH/7-1Ra and www.iaea.org/programmes/ripc/physics/fec2002/html/fec2002.htm
[19] Gorelenkov N.N., Fredrickson E., Belova E., Cheng C.Z., Gates D., Kaye S. and White R. 2003 Theory and observations of high frequency Alfvén eigenmodes in low aspect ratio plasmas *Nucl. Fusion* **43** 228
[20] Belova E., Gorelenkov N.N., Cheng C.Z. and Fredrickson E.D. 2003 Numerical study of instabilities driven by energetic neutral beam ions in NSTX *Proc. 30th European Physical Society Conf. on Controlled Fusion and Plasma Physics (St Petersburg, Russia, July 2003)* vol 27A (ECA) P-3.102
[21] Belikov V.S., Kolesnichenko Ya.I. and White R.B. 2003 Destabilization of fast magnetoacoustic waves by circulating energetic ions in toroidal plasmas *Phys. Plasmas* **10** 4771
[22] Fredrickson E.D., Gorelekov N.N. and Menard J. 2004 Phenomenology of compressional Alfvén eigenmodes *Phys. Plasmas* **11** 3653
[23] Gorelenkov N.N., Fredrickson E.D., Heidbrink W.W., Crocker N.A., Kubota S. and Peebles W.A. 2006 Discrete compressional Alfvén eigenmode spectrum in tokamaks *Nucl. Fusion* **46** S933
[24] Heidbrink W.W., Fredrickson E.D., Gorelenkov N.N., Rhodes T.L. and Van Zeeland M.A. 2006 Observation of compressional Alfvén eigenmodes (CAE) in a conventional tokamak *Nucl. Fusion* **46** 324
[25] Kolesnichenko Ya., White R.B. and Yakovenko Yu.V. 2006 High-frequency shear Alfvén instability driven by circulating energetic ions in NSTX *Phys. Plasmas* **13** 122503
[26] Berk H.L. *et al* and JET EFDA contributors 2006 Interpretation of mode frequency sweeping in JET and NSTX *Proc. 21st Int. Conf. on Fusion Energy 2006 (Chengdu, China, 2006)* (Vienna: IAEA) CD-ROM file TH/3-1 and http://www-naweb.iaea.org/napc/physics/FEC/FEC2006/html/index.htm
[27] Belova E.V., Gorelenkov N.N., Fredrickson E.D. and Bulletin of the American Physical Society 2009 Numerical modeling of NBI-driven GAE modes 2009 *APS April Meeting (Denver, Colorado, May 2009)* abstract #S1.070 (2009) and http://meetings.aps.org/ Meeting/APR09/PersonIndex/1382
[28] McClements K.G., Gryaznevich M.P., Sharapov S.E., Akers R.J., Appel L.C., Counsell G.F., Roach C.M. and Majeski R. 1999 *Plasma Phys. Control. Fusion* **41** 661
[29] Gryaznevich M.P. and Sharapov S.E. 2000 Frequency sweeping Alfvén instabilities driven by super-Alfvénic beams in the spherical tokamak START *Nucl. Fusion* **40** 907
[30] Appel L.C., Akers R.J., Martin R. and Pinfold T. 2004 Observation of CAEs on MAST *31st EPS Conf. on Plasma Physics (London, UK)* vol 28G (Ciità di Catelo, Perugia: Monotypia Franchi) P-4.198
[31] Pinches S.D., Berk H.L., Gryaznevich M.P. and Sharapov S.E. 2004 Spectroscopic determination of the internal amplitude of frequency sweeping TAE *Plasma Phys. Control. Fusion* **46** s47
[32] Sharapov S.E.*et al* 2005 Experimental studies of instabilities and confinement of energetic particles on JET and MAST *Nucl. Fusion* **45** 1168
[33] Gryaznevich M.P., Sharapov S.E., Berk H.L. and Pinches S.D. 2005 Alfven eigenmodes in spherical tokamaks *Trans.Inst. Electr. Eng. Japan* A **125-A** 908–13
[34] Vann R.G.L., Dendy R.O. and Gryaznevich M.P. 2005 Theoretical interpretation of frequency sweeping observations in the Mega-Amp Spherical Tokamak *Phys. Plasmas* **12** 032501
[35] Tournianski M.R., Akers R.J., Carolan P.G. and Keeling D.L. 2005 Anisotropic fast neutral particle spectra in the MAST spherical tokamak *Plasma Phys. Control. Fusion* **47** 671
[36] Gryaznevich M.P. and Sharapov S.E. 2006 Perturbative and non-perturbative modes in START and MAST *Nucl. Fusion* **46** S942
[37] Lilley M.K., Sharapov S.E., Smith H.M., Akers R.J., McCune D. and MAST team 2008 Modelling of beam-driven high frequency Alfvén eigenmodes in MAST

35th EPS Conf. on Plasma Physics (Crete, Greece, 2008) and http://epsppd.epfl.ch/Hersonissos/pdf/P1_057.pdf
[38] Appel L.C., T Fülöp, Hole M.J., Smith H.M., Pinches S.D., Vann R.G.L. and The MAST Team 2008 Compressional Alfvén Eigenmodes on MAST *Plasma Phys. Control. Fusion* **50** 115011
[39] Gryaznevich M.P. *et al* and the MAST Team 2008 Recent experiments on Alfvén eigenmodes in MAST *Nucl. Fusion* **48** 084003
[40] Kusama Y. *et al* 1999 Characteristics of Alfvén eigenmodes, burst modes and chirping modes in the Alfvén frequency range driven by negative ion based neutral beam injection in JT-60U *Nucl. Fusion* **39** 1837
[41] Saigusa M., Kimura H., Moriyama S., Neyatani Y., Fujii T., Koide Y., Kondoh T., Sato M., Nemoto M., Kamada Y. and JT-60 team 1995 Investigation of high-n TAE modes excited by minority-ion cyclotron heating in JT-60U *Plasma Phys. Control. Fusion* **37** 295
[42] Durst R.D., Fonck R.J., Wong K.L., Cheng C.Z., Fredrickson E.D. and Paul S.F. 1992 Measurements of the radial structure and poloidal spectra of toroidal Alfvén eigenmodes in the Tokamak Fusion Test Reactor *Phys. Fluids* B **4** 3707
[43] Chang Z. *et al* and the TFTR Group 1997 Alpha-driven magnetohydrodynamics (MHD) and MHD-induced alpha loss in the Tokamak Fusion Test Reactor *Phys. Plasmas* **4** 1610
[44] Heidbrink W.W., Strait E.J., Doyle E., Sager G. and Snider R.T. 1991 An investigation of beam driven Alfvén instabilities in the DIII-D tokamak *Nucl. Fusion* **31** 1635
[45] Heidbrink W.W. *et al* 2008 Central flattening of the fast-ion profile in reversed-shear DIII-D discharges *Nucl. Fusion* **48** 084001
[46] Ali-Arshad S. and Campbell D.J. 1995 Observation of TAE activity in JET *Plasma Phys. Control. Fusion* **37** 715
[47] Fasoli A., Testa D., Sharapov S., Berk H.L., Breizman B., Gondhalekar A., Heeter R.F. and Mantsinen M. 2002 MHD Spectroscopy *Plasma Phys. Control. Fusion* **44** B159–72
[48] Garcia-Munoz M. *et al* and the ASDEX Upgrade Team 2011 Fast-ion transport induced by Alfvén eigenmodes in the ASDEX Upgrade tokamak *Nucl. Fusion* **51** 103013
[49] Lauber Ph., Brüdgam M., Curran D., Igochine V., Sassenberg K., Günter S., Maraschek M., García-Muñoz M., Hicks N. and the ASDEX Upgrade Team 2009 Kinetic Alfvén eigenmodes at ASDEX Upgrade *Plasma Phys. Control. Fusion* **51** 124009
[50] Fredrickson E.D. *et al* 2012 Observation of global Alfvén eigenmode avalanche events on the National Spherical Torus Experiment *Nucl. Fusion* **52** 043001
[51] White R.B. and Chance M.S. 1984 *Phys. Fluids* **27** 2455
[52] Cheng C.Z. 1992 Kinetic extensions of magnetohydrodynamic models for axisymmetric toroidal plasmas *Phys. Rep.* **211** 1–51
[53] Kramer G.J. *et al* 2006 Interpretation of core localized Alfvén eigenmodes in DIII-D and Joint European Torus reversed magnetic shear plasmas *Phys. Plasmas* **13** 056104
[54] Carolipio E.M., Heidbrink W.W., Cheng C.Z., Chu M.S., Fu G.Y., Jaun A., Spong D.A., Turnbull A.D. and White R.B. 2001 The toroidicity-induced Alfvén eigenmode structure in DIII-D: Implications of soft x-ray and beam-ion loss data *Phys. Plasmas* **8** 3391
[55] White R.B., Gorelenkov N., Heidbrink W.W. and Van Zeeland M.A. 2010 Particle distribution modification by low amplitude modes *Plasma Phys. Control. Fusion* **52** 045012
[56] Todo Y., Berk H.L. and Breizman B.N. 2003 Simulation of intermittent beam ion loss in a Tokamak Fusion Test Reactor experiment *Phys. Plasmas* **10** 2888
[57] Lang J., Fu G.-Y. and Chen Y. 2010 Nonlinear simulation of toroidal Alfvén eigenmode with source and sink *Phys. Plasmas* **17** 042309
[58] Fredrickson E.D. *et al* 2009 Modeling fast-ion transport during toroidal Alfvén eigenmode avalanches in National Spherical Torus Experiment *Phys. Plasmas* **16** 122505
[59] Budny R.V. 2002 Fusion alpha parameters in tokamaks with high DT fusion rates *Nucl. Fusion* **42** 1383
[60] Levinton F.M. and Yuh H. 2008 *Rev. Sci. Instrum.* **74** 10F522
[61] Levinton F.M. *et al* 2007 Transport with reversed shear in the National Spherical Torus Experiment *Phys. Plasmas* **14** 056119
[62] Budny R.V. 1994 *Nucl. Fusion* **34** 1247
[63] Crocker N.A. *et al* 2011 High spatial sampling global mode structure measurements via multichannel reflectometry in NSTX *Plasma Phys. Control. Fusion* **53** 105001
[64] Huba J.D. 1994 NRL Plasma Formulary Naval Research Laboratory, Washington DC, p 45
[65] Fisch N.J. and Rax J.-R. 1992 *Phys. Rev. Lett.* **69** 612